Chapter 2

Generation of coherence in an exactly solvable nonlinear nanomechanical system

2.1 Introduction

Experimental advances in fabrication and characterization of a nano-electromechanical systems (NEMS), quantum opto-electromechanics, cavity quantum electrodynamics gave further impetus to the fields of quantum computation and quantum hybrid systems [26, 27, 28, 29, 152, 153, 154, 155, 156, 157, 158, 159, 160, 161, 162, 163, 164, 165, 166, 167, 168, 169, 170, 171, 172, 173, 174]. NEMS as hybrid systems are important for quantum information transfer, and to facilitate entanglement [175], and also serve for studying fundamental questions at the quantum-classical boundaries. Key features of NEMS are the high Q-factors, low masses and the high frequency of the mechanical oscillations (of the order of Gigahertz (GHz)) [176]. Recently, entangling two micro-mechanical oscillators has been achieved [61]. Efficient experimental implementation of quantum control has also been achieved using a quantum opto-electro-mechanical protocol[62]. With ground-

state cooling [177, 178] exploring the quantum nature of the mechanical motion becomes feasible. Furthermore, the coupling of a nanomechanical resonator to a nearby (quantum) spin was studied [63]. In addition, on the basis of these hybrid systems various realizations of qubits were proposed and realized. One such system is a NV-center, which is a nitrogen vacancy defect in a diamond lattice. The researchers in this area are mainly interested in the dynamics of the NV center that can be described effectively by a spin-1 system with a large decoherence time. The Hamiltonian of the NV center couples the ground state $|0\rangle$ to a bright superposition of excited states $|b\rangle = \frac{1}{\sqrt{2}}(|-1\rangle + |1\rangle)$, while the "dark" superposition $|d\rangle = \frac{1}{\sqrt{2}}(|-1\rangle - |1\rangle)$ remains decoupled [172]. This allows to map the NV centers in external microwave driving onto a pseudospin 1/2 system.

As follows from the Ehrenfest's theorem, for a system subjected to a potential $V(\{q_g\})$ with $\langle V(\{q_g\})\rangle = V(\langle\{q_g\}\rangle)$ (where $\langle\cdots\rangle$ is the quantum mechanical average and $\{q_g\}$ stands for generalized coordinates), the dynamics of a quantum observable follows its classical counterpart. However, on a time scale larger than the Ehrenfest time, classical nonlinear system and it's quantum counterpart manifest different features [179].

We note that the nonlinear phenomenon plays an incisive role for NEMS. Effects such as Kerr-like nonlinearity [180, 181] for mechanical resonators or the phononic nonlinear regime in strong external fields becomes relevant [182, 183]. Traditionally, in physics and mathematics, classical nonlinear systems have been studied intensively as they show a wide range of interesting phenomena [184], that are expected to be reflected in the quantum behavior when such classical systems are coupled to quantum ones. For instance, Drummond and Walls [185] showed that a nonlinear model of an optical cavity being driven by a continuous external field shows a bistable window in its semiclassical description. This can be contrasted with an analogous quantum system in which bistable regime is not present.

In this chapter we investigate a paradigmatic model of NEMS hybrid system: a nonlinear oscillator coupled to a spin 1/2 system. We show that in spite of the nonlinearity in the system, the exact analytical solution is accessible. We introduce a scheme of periodic driving and study the combined effects of the driving and coupling between the spin and the nonlinear oscillator. The advantage of the NV centers is their relatively low decoherence rate. However, on the longer run, even a low decoherence may lead to substantial effects. Thus, we use a simple unitary evolution protocol which (even though not reducing entirely the decoherence) leads to the generation of coherence.

The chapter is divided into the sections as follows: In Section-2.2, we discuss the model and transformation of the cantilever problem to a mathematical pendulum. In Section-2.3, we formulate the Mathieu Schrödinger equation. Next, in section-2.4, we discuss the spin dynamics of the NV center. Subsequently, in section 2.5, we study the effects of the environment with a Lindblad master equation and non-Markovian noise due to ^{13}C nuclei in the surroundings of NV spin. Section-2.6 is about multilevel dynamics and entanglement, followed by Section-2.7 that addresses the unitary generation of coherence. Section 2.8 summarizes.

2.2 Theoretical modeling

The Hamiltonian of the NV center coupled to a driven nonlinear oscillator reads [173]

$$H\left(x,p,t\right) \;=\; H_S + H_0\left(x,p\right) + H_{NL} + \varepsilon V\left(x,t\right) + g\cos(\omega t)xS_z. \tag{2.1}$$

Here $H_s = \frac{1}{2}\omega_0\sigma_z$ is the Hamiltonian of the NV center, $\omega_0 = \left(\omega_R^2 + \delta^2\right)^{1/2}$, ω_R is the Rabi frequency, and δ is the detuning between the microwave frequency and the intrinsic frequency of the spin. In what follows,we set $\hbar$ equal to one. The operator S_z in the eigenbasis of the NV center has the form: $S_z = \frac{1}{2}\left(\cos(\alpha)\sigma_z + \sin(\alpha)(\sigma_+ + \sigma_-)\right)$ with

$\tan(\alpha) = -\omega_R/\delta$ and $\sigma_z = |e\rangle\langle e| - |g\rangle\langle g|$, $\sigma_+ = |e\rangle\langle g|$, $\sigma_- = |g\rangle\langle e|$. For more details see [173]. The terms H_0 and H_{NL} represent linear and nonlinear parts of the oscillator respectively:

$$H_0 = \frac{p^2}{2m} + \frac{\omega_r^2 m x^2}{2}, \quad H_{NL} = \beta x^3 + \mu x^4, \tag{2.2}$$

where ω_r is the frequency of the oscillations, β and μ are constants of the nonlinear terms. The term

$$V(x,t) = V_0 x \cos\omega t, \quad \varepsilon V_0 = f_0, \quad \varepsilon \ll 1. \tag{2.3}$$

describes the driven motion of the cantilever in the RF field with frequency ω. The last term in Eq. (2.1) describes the coupling between the oscillator and the NV spin. The distance and the coupling strength between the magnetic tip and NV spin can be modulated through the magnetostriction effect [174].

Our description of the problem is quite general. However, without the loss of generality we specify the values of the parameters relevant for the NV centers[172]: $\frac{\omega_r}{2\pi} = 5$ MHz, $\frac{\omega_R}{2\pi} = 0.1 - 10$ MHz, $\delta = 1$ kHz, mass of the cantilever $m = 6 \times 10^{-17}$ kg, the coupling constant $\frac{g}{2\pi} = 100$ kHz, the amplitude of the zero point fluctuations $a_0 = \sqrt{\hbar/2m\omega_r} \approx 5 \times 10^{-3}$ m. The nonlinear constants are order of $\beta \approx \frac{\omega_r^2 m}{2a_0}$, $\mu \approx \frac{\omega_r^2 m}{2a_0^2}$. The energy scale of the problem is defined by $\varepsilon V \approx \omega_r^2 m a_0^2 \approx 10^{-9}$J, and the time scale is of order of microsecond scale $t \approx \frac{\pi}{2g}$ microseconds.

2.2.1 Classical cantilever dynamics

Let us discuss the dynamics of classical nonlinear cantilever using the Hamiltonian given by Eqs. (2.2) and (2.3). The equation of motion governed by $H_0 + H_{NL} + V(x,t)$ has the form:

$$\ddot{x} + \omega_r^2(1 + \alpha_3 x + \alpha_4 x^2)x = V_0 \cos(\omega t). \tag{2.4}$$

For brevity we introduced the notations $\alpha_3 = 3\beta/\omega_r^2, \quad \alpha_4 = 4\mu/\omega_r^2$. Adopting the perturbation ansatz

$$x(t) = x^{(1)}(t) + x^{(2)}(t) + x^{(3)}(t) + \cdots, \; x^{(1)}(t) = V_0 \cos(\Omega t),$$

where

$$\Omega = \omega_r + \Omega_1 + \Omega_2 + \cdots,$$

the equation (2.4) now takes on the form:

$$\big(\omega_r/\Omega\big)^2 \ddot{x} + \omega_r^2 x \;\; = \;\; -\alpha_3 \omega_r^2 x^2 - \alpha_4 \omega_r^2 x^3 - \big(1 - \omega_r^2/\Omega\big)\ddot{x} + V_0 \cos(\omega t). \tag{2.5}$$

Suppose that $\omega = \omega_r/3 + \Delta\Omega$, where $\Delta\Omega$ is the small modulation frequency in the vicinity of the resonance $n\Omega(x) \approx m\omega$, where $n, \; m \in \mathbb{Z}$. Then the first order term $x^{(1)}(t) \sim \cos\big[3\big(\omega_r/3 + \Delta\Omega\big)\big]$ is off-resonance. However, the second-order term $\{x^{(1)}(t)^3\} \sim \cos\big[3\big(\omega_r/3 + \Delta\Omega\big)\big]$ already leads to the parametric resonance. For our convenience we switch to the canonical pair of action-angle (I, θ) variables. The cantilever part of the Hamiltonian $H_{p,q} = H_0 + H_{NL} + V(x,t)$ expressed in new variables $H_{I,\theta}$ is connected to the original Hamiltonian through the production function $\Phi = F + I\theta$ via the relation:

$$d\Phi = pdq + \theta dI + \big(H_{I,\theta} - H_{p,q}\big)dt, \tag{2.6}$$

and the canonical set of equations in new variables are:

$$\left.\begin{aligned} \frac{dI}{dt} &= -\frac{\partial H_{I,\theta}}{\partial \theta} = -\varepsilon \frac{\partial V(I,\theta,\lambda)}{\partial \theta}, \\ \frac{d\theta}{dt} &= \frac{\partial H_{I,\theta}}{\partial I} = \Omega(I) + \varepsilon \frac{\partial V(I,\theta,\lambda)}{\partial I}. \end{aligned}\right\} \tag{2.7}$$

Here we introduced the nonlinear frequency $\Omega(I) = \partial(H_0 + H_{NL})/\partial I$ and $\dot{\lambda} = \omega$ the frequency of external driving. Nonlinearity of the system is quantified by the following

criterion:

$$\begin{aligned}\mathscr{A} &= \left|\frac{I}{\Omega(I)}\frac{d\Omega(I)}{dI}\right| \\ &= \left|I\left(\frac{\partial(H_0+H_{NL})}{\partial I}\right)^{-1}\frac{d}{dI}\left(\frac{\partial(H_0+H_{NL})}{\partial I}\right)\right|. \end{aligned} \tag{2.8}$$

where,

$$H_0(I) = \omega_r I + H_{NL}, \quad H_{NL} = 3\pi\left(\frac{I}{m\omega_r}\right)^2\mu. \tag{2.9}$$

The deviation of action from the resonance value is given by $\Delta I = I - I_0$. The nonlinear frequency $\Omega(I) = \partial H_0/\partial I + \partial H_{NL}/\partial I$ and the nonlinear resonance condition in the action-angle variables has the form $\omega_r + \Omega_{NL}(I_0) = \omega$, $\Omega_{NL} = 6\pi I(\mu/m^2\omega_r^2)$.

Our method is valid if $1/\varepsilon \gg \mathscr{A} \gg \varepsilon$ [186]. To explore the nonlinear multiple resonances, we utilize the standard expansion adopted in the theory of dynamical systems [186]

$$\varepsilon V(I,\theta,\lambda) = \frac{1}{2}\sum_{n,m} V_{n,m}(I)\exp\left[i(m\lambda + n\theta)\right] + c.c. \tag{2.10}$$

and insert Eq. (2.10) in Eq. (2.8) to find

$$\left.\begin{aligned}\frac{dI}{dt} &= \varepsilon n V_{mn}\sin(F_{mn}), \\ \frac{dF_{mn}}{dt} &= m\omega + n\Omega(I) + \varepsilon n\left(\frac{\partial V_{mn}}{\partial I}\right)\cos(F_{mn}).\end{aligned}\right\} \tag{2.11}$$

Here $F_{mn} = m\lambda + n\theta$ is the resonant phase. Let I_0 correspond to the exact resonance $F_{mn} = 0$, $|\triangle I - I_0| = |\triangle I| \ll I_0$. The set of equations Eq. (2.11) for the deviation of the

action $\triangle I$ becomes

$$\left.\begin{aligned}\frac{d(\triangle I)}{dt} &= \varepsilon n V_{mn}\sin(F_{mn}),\\ \frac{d(F_{mn})}{dt} &= n\big[\Omega(I)-\Omega(I_0)\big]\\ &\quad+\varepsilon n\left[\frac{\partial V_{mn}}{\partial I}\cos(F_{mn})-\frac{\partial V_{mn}(I_0)}{\partial I}\right].\end{aligned}\right\} \tag{2.12}$$

Taking into account that $\Omega(I)-\Omega(I_0)\approx\left(\frac{\partial\Omega}{\partial I}\right)_{I=I_0}\triangle I=\mathscr{A}\Omega(I_0)\triangle I/I_0$ and the condition of the moderate nonlinearity $1/\varepsilon\gg\mathscr{A}\gg\varepsilon$, in Eq. (2.12) , we find:

$$\left.\begin{aligned}\frac{d\triangle I}{dt} &= \varepsilon n V_{mn}\sin(F_{mn}),\\ \frac{dF_{mn}}{dt} &= n\left(\frac{\partial\Omega(I)}{\partial I}\right)_{I=I_0}.\end{aligned}\right\} \tag{2.13}$$

These are the Hamilton's equations with the Hamiltonian

$$H_{I,\theta}=n\left(\frac{d\Omega(I)}{dI}\right)_{I_0}\frac{(\triangle I)^2}{2}+\varepsilon n V_{mn}(I_0)\cos(F_{mn}). \tag{2.14}$$

For simplicity we use the rotating wave approximation and retain the slow phase in the oscillator-spin coupling term $\varphi=\theta-\omega t$. Considering only the first resonance $n=m=1$ from Eq. (2.1) we deduce the transformed total Hamiltonian as

$$H=H_s+H_0(I)+\big\{\varepsilon V(I)+Q(I)S_z\big\}\cos(\varphi). \tag{2.15}$$

Here, for brevity, the following notations are used

$$\varepsilon V(I)=V_0\sqrt{I/m\omega_r},\ Q(I)=g\sqrt{I/m\omega_r}. \tag{2.16}$$

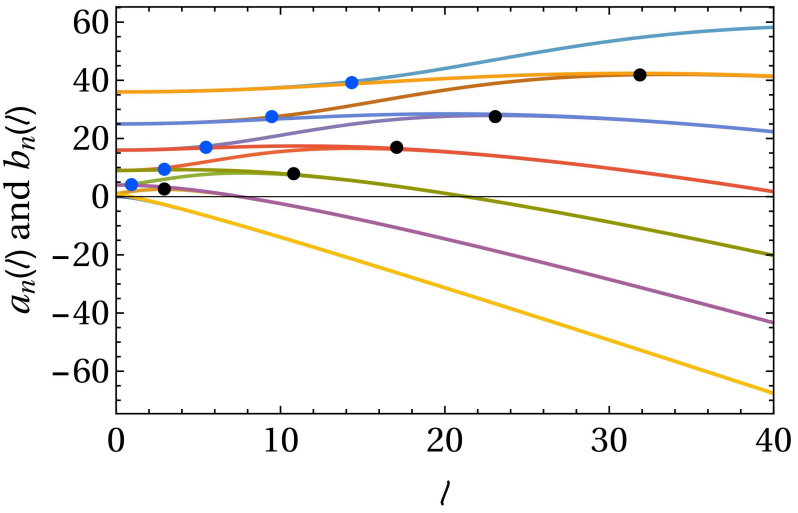

Fig. 2.1 Energy spectrum $E_n(l)$ of Mathieu-Schrödinger equation with varying barrier height l. The region where curves are split is called G_0 and the merging points define the boundaries of the G_- and G_+ subgroups. The energy spectrum corresponding to Mathieu function $|ce_n(l,\varphi)\rangle$ is described by Mathieu characteristic $a_n(l)$, and the energy spectrum corresponding to Mathieu function $|se_n(l,\varphi)\rangle$ is described by Mathieu characteristic $b_n(l)$. Barrier height l is in units of $\frac{U}{\omega'}$.

2.3 Quantum cantilever dynamics

The transformed Hamiltonian of Eq. (2.1) can be written as

$$H = H_m + H_s + Q\cos\varphi S_z, \tag{2.17}$$

where H_m is the Hamiltonian of a mathematical pendulum given by

$$H_m = \frac{\omega'}{2}\left(\triangle I\right)^2 + U\cos\varphi, \tag{2.18}$$

with the notations $\omega' = \left(d\Omega_{NL}(I)/dI\right)|_{I=I_0}$, $U = \varepsilon V\left(I_0\right)$. We are interested in the analytical solutions to the Hamiltonian Eq. (2.18). The Schrödinger equation with the Hamiltonian H_m, is related to corresponding Mathieu-Schrödinger equation and its spectrum. This becomes evident when applying correspondence principle, by relating the classical variables to the corresponding operators, meaning $\Delta I \to \imath\hbar\partial/\partial\varphi$ in Eq. (2.18) which relates the

Hamiltonian of the mathematical pendulum H_m to the Mathieu-Schrödinger equation

$$\frac{d^2\psi_n}{d\varphi^2} + \big(E_n - 2l\cos 2\varphi\big)\psi_n = 0. \tag{2.19}$$

The effective potential is $V(l,\varphi) = 2l\cos 2\varphi$, and rescaled energy, the potential barrier and the angle are $E_n \to \frac{8E_n}{\omega'}$, $l \to \frac{8U}{\omega'}$, $\varphi \to 2\varphi$, respectively.

A detailed analysis of the Mathieu-Schrödinger equation (2.19) was done in numerous works, for example the references [187, 188, 189, 190]. The energy spectrum of the Mathieu-Schrödinger equation depends parametrically on the potential barrier $E_n\big(l\big)$ and contains two degenerate G_-, G_+ and one non-degenerate domain G_0 (See Fig. 2.1). The eigenfunctions of each region G_-, G_+ and G_0 are the basis functions of the irreducible representations of the invariant subgroups of Klein's four-group:

$$\begin{aligned} &G_0 \subset \mathscr{E}, \mathscr{A}, \\ &G_- \subset \mathscr{E}, \mathscr{C}, \\ &G_+ \subset \mathscr{E}, \mathscr{B}. \end{aligned} \tag{2.20}$$

and the group elements are

$$\begin{aligned} &G\big(\varphi \to -\varphi\big) = \mathscr{A}, \quad G\big(\varphi \to \pi - \varphi\big) = \mathscr{B}, \\ &G\big(\varphi \to \pi + \varphi\big) = \mathscr{C}, \quad G\big(\varphi \to \varphi\big) = \mathscr{E}, \end{aligned} \tag{2.21}$$

while the irreducible basis functions for each subgroup are defined explicitly in Eq.(1.14) to Eq.(1.16).

where, $ce_n(l,\varphi)$ and $se_n(l,\varphi)$ are Mathieu functions with characteristic values $a_n(l)$ and $b_n(l)$, respectively. The trigonometric series representation of Mathieu functions [97] are also shown in Eq.(1.17) to Eq.(1.20).

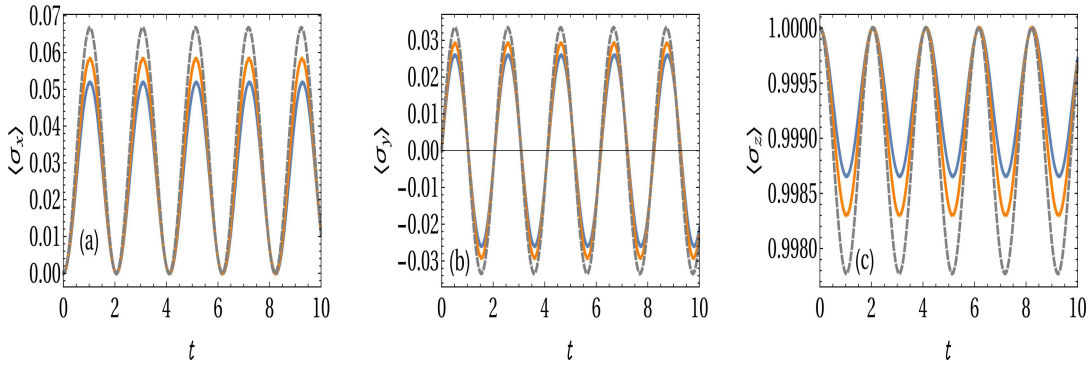

Fig. 2.2 (a) Average transverse spin component $\langle\sigma_x\rangle$, (b) average transverse spin component $\langle\sigma_y\rangle$, and (c) average longitudinal spin component $\langle\sigma_z\rangle$, plotted for the bipartite system $\hat{\rho}_{AB}$ in the region G_0 for different quantum numbers $n = 2,3,4$. In all the figures blue (solid), orange (solid) and violet (dashed) lines represent $n = 2, l = 3.855$, $n = 3, l = 7.535$ and $n = 4, l = 10.785$ cases, respectively. The values of the barrier heights l are chosen to be in G_0 region for the given n. The interaction strength between the nonlinear oscillator and the NV spin is taken to be $Q = 0.5$. Time is in the units of ω_0^{-1}, which is of the order of nanoseconds.

2.4 Quantum spin dynamics of NV center

The system of the nonlinear oscillator coupled with the NV center spin is transformed into a system of a mathematical pendulum coupled with the NV center spin. In the previous section we have found the eigenfunctions and eigenvalues of the mathematical pendulum in terms of the Mathieu functions and the characteristic values of the Mathieu-Schrödinger equation. To explore the total Hamiltonian $\hat{H}$, Eq.(2.18) we use the joint basis of eigenfunctions of the mathematical pendulum Eq.(1.14)-Eq. (1.16) and the basis functions of Pauli matrix σ_z for the spin part *i.e.,* $|\chi\rangle \equiv \{|1\rangle,\ |0\rangle\}$. The total Hamiltonian Eq. (2.17) reads

$$\hat{H} = \begin{pmatrix} A_{11} & A_{12} & A_{13} & A_{14} \\ A_{21} & A_{22} & A_{23} & A_{24} \\ A_{31} & A_{32} & A_{33} & A_{34} \\ A_{41} & A_{42} & A_{43} & A_{44} \end{pmatrix}, \tag{2.22}$$

where the matrix elements A_{ij} for the region G_-, G_0 and G_+ are presented in the Appendix A . S-I. In the region G_0, for a given quantum number n, the system can be found either

in the states $|ce_n(\varphi,l)\rangle \otimes |0\rangle$ and $|ce_n(\varphi,l)\rangle \otimes |1\rangle$, or in the states $|se_n(\varphi,l)\rangle \otimes |0\rangle$ and $|se_n(\varphi,l)\rangle \otimes |1\rangle$. We note that these states correspond to a particular fixed quantum number n. The presence of the spin-oscillator coupling term leads to the mixing of the nonlinear oscillator states. However, when the distance between the neighbor states is larger than the spin-oscillator coupling strength $E_{n+1} - E_n > g$, the states with a different quantum number are eliminated from the process. Suppose that the system is in the states $|ce_n(\varphi,l)\rangle \otimes |0\rangle$ and $|ce_n(\varphi,l)\rangle \otimes |1\rangle$, then the Hamiltonian of the system in G_0 region can be written as:

$$\hat{H} = \begin{pmatrix} a_n(l) + \frac{1}{2}\omega_0 + \frac{1}{2}Qe\cos\alpha & \frac{1}{2}Qe\sin\alpha \\ \frac{1}{2}Qe\sin\alpha & a_n(l) - \frac{1}{2}\omega_0 - \frac{1}{2}Qe\cos\alpha \end{pmatrix}. \tag{2.23}$$

The eigenvalues of the above Hamiltonian (2.23) are $a \pm \sqrt{b^2+c^2}$ and the corresponding eigenvectors are $|\phi_1\rangle = |ce_n\rangle(\alpha_1|1\rangle + \beta_1|0\rangle)$, $|\phi_2\rangle = |ce_n\rangle(\beta_1|1\rangle - \alpha_1|0\rangle)$, where $\alpha_1 = 1/\sqrt{\lambda^2+1}$, $\beta_1 = \lambda/\sqrt{\lambda^2+1}$, $\lambda = (b+\sqrt{b^2+c^2})/c$, $a = a_n(l)$ is the energy spectrum corresponding to Mathieu function $|ce_n(l,\varphi)\rangle$, $b = \frac{1}{2}\omega_0 + \frac{1}{2}Qe\cos\alpha$, $c = \frac{1}{2}Qe\sin\alpha$ and

$$e = \{\frac{\pi}{2}\left(A_1^{(2n+1)}(l)\right)^2 + \pi\sum_{r=0}^{\infty} A_{2r+1}^{(2n+1)}(l)A_{2r+3}^{(2n+1)}(l)\}. \tag{2.24}$$

If the system is in the state $|se_n(\varphi,l)\rangle \otimes |0\rangle$ and $|se_n(\varphi,l)\rangle \otimes |1\rangle$, the Hamiltonian is

$$\hat{H} = \begin{pmatrix} b_n(l) + \frac{1}{2}\omega_0 + \frac{1}{2}Qf\cos\alpha & \frac{1}{2}Qf\sin\alpha \\ \frac{1}{2}Qf\sin\alpha & b_n(l) - \frac{1}{2}\omega_0 - \frac{1}{2}Qf\cos\alpha \end{pmatrix}. \tag{2.25}$$

The eigenvalues and corresponding eigenvectors in this case are $a_x \pm \sqrt{[b_x^2+c_x^2]}$ and $\left[\lambda_x/\sqrt{\lambda_x^2+1}, 1/\sqrt{\lambda_x^2+1}\right]$, $\lambda_x = (b_x \pm \sqrt{[b_x^2+c_x^2]})/c_x$

Where $a_x = b_n(l)$ is the energy spectrum corresponding to Mathieu function $|se_n(l,\varphi)\rangle$,

$b_x = \frac{1}{2}\omega_0 + \frac{1}{2}Qf\cos\alpha$, $c_x = \frac{1}{2}Qf\sin\alpha$, and

$$f = \{\frac{\pi}{2}\left(-B_1^{(2n+1)}(l)\right)^2 + \pi\sum_{r=0}^{\infty} B_{2r+1}^{(2n+1)}(l)B_{2r+3}^{(2n+1)}(l)\}. \tag{2.26}$$

Similarly in the degenerate G_- region the total Hamiltonian (2.22) takes the form:

$$\hat{H} = \begin{pmatrix} a_- + b_1 & e_1 & c_1 & d_1 \\ e_1 & a_- - b_1 & d_1 & -c_1 \\ c_1 & d_1 & a_+ + b_1 & e_1 \\ d_1 & -c_1 & e_1 & a_+ - b_1 \end{pmatrix}, \tag{2.27}$$

where $a_\mp = a_1 = a_n(l) + b_n(l)$, $b_1 = \frac{1}{2}\omega_0 + \frac{1}{4}Qr\cos\alpha$, $c_1 = \frac{1}{4}f_1Q\cos\alpha$, $d_1 = \frac{1}{4}f_1Q\sin\alpha$, $e_1 = \frac{1}{4}Qr\sin\alpha$,

$$\begin{aligned} r &= \left[\{\frac{\pi}{2}\left(A_1^{(2n+1)}(l)\right)^2 + \pi\sum_{r=0}^{\infty} A_{2r+1}^{(2n+1)}(l)A_{2r+3}^{(2n+1)}(l)\} + \{\frac{\pi}{2}\left(-B_1^{(2n+1)}(l)\right)^2\right. \\ &+ \left.\pi\sum_{r=0}^{\infty} B_{2r+1}^{(2n+1)}(l)B_{2r+3}^{(2n+1)}(l)\}\right], \end{aligned} \tag{2.28}$$

$$\begin{aligned} f_1 &= \left[\{\frac{\pi}{2}\left(A_1^{(2n+1)}(l)\right)^2 + \pi\sum_{r=0}^{\infty} A_{2r+1}^{(2n+1)}(l)A_{2r+3}^{(2n+1)}(l)\} + \{\frac{\pi}{2}\left(-B_1^{(2n+1)}(l)\right)^2\right. \\ &+ \left.\pi\sum_{r=0}^{\infty} B_{2r+1}^{(2n+1)}(l)B_{2r+3}^{(2n+1)}(l)\}\right]. \end{aligned} \tag{2.29}$$

Four eigenvalues of the above Hamiltonian are

$$a_1 \pm \sqrt{[b_1^2 - 2b_1c_1 + c_1^2 + d_1^2 - 2d_1e_1 + e_1^2]}, \tag{2.30}$$

and

$$a_1 \pm \sqrt{[b_1^2 + 2b_1c_1 + c_1^2 + d_1^2 + 2d_1e_1 + e_1^2]}. \tag{2.31}$$

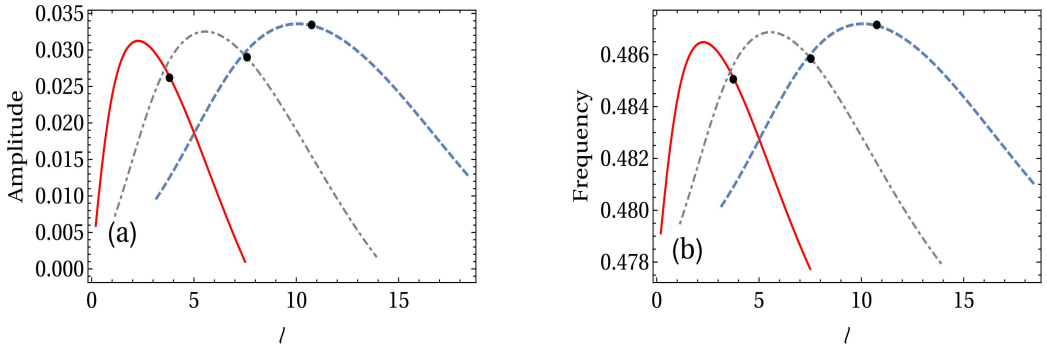

Fig. 2.3 (a) The amplitude and (b) frequency of $\langle\sigma_x\rangle$ with respect to barrier height l for different values of n. The quantum numbers n and l are chosen such that the mathematical pendulum remains in G_0 region. In all the figures, red (solid), violet (Dot-Dashed) and blue (dashed) lines represent $n=2$, $n=3$ and $n=4$ cases, respectively. The dots in the figures represent the points which are considered in Fig. 2.2. Barrier height l is in units of $\frac{U}{\omega'}$.

The explicit form of the eigenvector corresponding to G_- region is given in Appendix A . S-II.

Let us assume that the system is initially in the G_0 region and the state of the system is given by

$$|\psi(0)\rangle = |ce_n(\varphi,l)\rangle \otimes |0\rangle. \tag{2.32}$$

The state of the system at any time t, $|\psi(t)\rangle$ is the solution of the Schrödinger equation using Hamiltonian Eq.(2.23):

$$i\hbar\frac{d|\psi(t)\rangle}{dt} = \hat{H}|\psi(t)\rangle. \tag{2.33}$$

To solve Eq. (2.33) one may use the ansatz

$$|\psi(t)\rangle = C_1(t)|ce_n(\varphi,l)\rangle|0\rangle + C_2(t)|ce_n(\varphi,l)\rangle|1\rangle. \tag{2.34}$$

The coefficients $C_1(t)$, $C_2(t)$ follow from Eqs.(2.33), (2.34). The density matrix at any time t can be calculated as $\rho_{AB}(t) = |\psi(t)\rangle\langle\psi(t)|$, A and B are used to emphasize the

bipartite character of the system consisting of the pendulum (A) and the spin parts (B). We trace out the subsystem of the mathematical pendulum $\rho_B = Tr_A \rho_{AB}(t)$ and the reduced density matrix is only the spin subsystem which is presented in a matrix form as

$$\rho_B(t) = \begin{pmatrix} \rho_{11} & \rho_{12} \\ \rho_{21} & \rho_{22} \end{pmatrix}. \tag{2.35}$$

The elements of the density matrix are given by:

$$\rho_{11} = \frac{b^2 + c^2(\cos\sqrt{b^2+c^2}t)^2}{(b^2+c^2)}, \tag{2.36}$$

$$\begin{aligned} \rho_{12} &= \rho_{21}^* \\ &= \frac{c(b - b\cos 2\sqrt{b^2+c^2}t - i\sqrt{b^2+c^2}\sin 2\sqrt{b^2+c^2}t)}{2(b^2+c^2)}, \end{aligned} \tag{2.37}$$

and

$$\rho_{22} = \frac{c^2(\sin^2\sqrt{b^2+c^2}t)}{(b^2+c^2)}. \tag{2.38}$$

Obviously, the state described by Eq. (2.34) is a pure state. Therefore, the purity that is defined as $\mathscr{P} = Tr(\rho_B^2) = 1$ and quantifies the mixedness between the pendulum and the spin subsystem is equal to one. We explore the dynamics of the expectation components of the spin $\langle\sigma_\alpha\rangle = Tr(\hat{\rho}\sigma_\alpha)$, $\alpha = x, y, z$ and deduce

$$\langle\sigma_z\rangle_{G_0} = \frac{b^2 + c^2\cos 2\sqrt{b^2+c^2}t}{b^2+c^2}, \tag{2.39}$$

$$\langle\sigma_y\rangle_{G_0} = \frac{c\sin 2\sqrt{b^2+c^2}t}{\sqrt{b^2+c^2}}, \tag{2.40}$$

$$\langle\sigma_x\rangle_{G_0} = \frac{2bc\sin^2\sqrt{b^2+c^2}t}{b^2+c^2}. \tag{2.41}$$

In Fig. 2.2 (a), (b) and (c) we show time evolution of $\langle\sigma_x\rangle_{G_0}$, $\langle\sigma_y\rangle_{G_0}$ and $\langle\sigma_z\rangle_{G_0}$ for different quantum states $n = 2$, 3 and 4. The quantum number l which characterizes the barrier height is chosen carefully so that the system is near the separatrix line defined as $E_n = l$ in the G_0 region for given value of n. From the above expressions of $\langle\sigma_x\rangle_{G_0}$, $\langle\sigma_y\rangle_{G_0}$ and $\langle\sigma_z\rangle_{G_0}$ it is evident that the modulation depth depends on b and c which varies with quantum numbers n and l through e. When the system is close to the separatix line the amplitude of the oscillations of transverse and longitudinal components of magnetization increases with increasing n and the frequency of oscillation remains constant. Let us include even those points of G_0 region which are away from the separatrix line corresponding to the given n. The amplitude of oscillations, for instance, for $\langle\sigma_x\rangle_{G_0}$ is given by $\frac{bc}{b^2+c^2}$, which follows a bell-shaped pattern as shown in Fig. 2.3 (a) for different values of n. The frequency of oscillation shows a similar behaviour as displayed in Fig. 2.3 (b). We can observe a similar trend for $\langle\sigma_y\rangle_{G_0}$ and $\langle\sigma_z\rangle_{G_0}$ cases.

The dynamics of the system in the subgroup G_- is much more complex. Let us consider the system initially in G_- region and the state of the system is given as

$$|\psi(0)\rangle = |\phi_n^-(\varphi,l)\rangle \otimes |0\rangle. \tag{2.42}$$

The state of the system at any time t can be obtained using the Eq. (2.33). We consider the following ansatz for the state of the system in the region G_-:

$$\begin{aligned} |\psi(t)\rangle &= \zeta_1(t)|\phi_n^-(\varphi,l)\rangle|0\rangle + \zeta_2(t)|\phi_n^-(\varphi,l)\rangle|1\rangle \\ &+ \zeta_3(t)|\phi_n^+(\varphi,l)\rangle|0\rangle + \zeta_4(t)|\phi_n^+(\varphi,l)\rangle|1\rangle. \end{aligned} \tag{2.43}$$

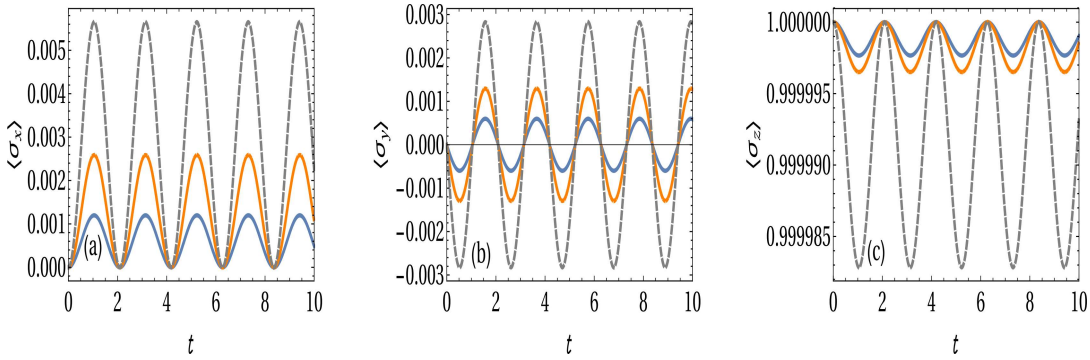

Fig. 2.4 (a) Average transverse spin component $\langle\sigma_x\rangle$, (b) average transverse spin component $\langle\sigma_y\rangle$, and (c) average longitudinal spin component $\langle\sigma_z\rangle$, plotted as a function of time for the bipartite system $\hat{\rho}_{AB}$ in the region G_- for different quantum numbers $n = 2,3,4$. In all the figures blue (solid), orange (solid) and violet (dashed) lines represent $n = 2, l = 0.1$, $n = 3, l = 0.57$ and $n = 4, l = 1.585$ cases, respectively. In all the cases the coupling constant Q is equal to 0.5. The values of barrier heights l are chosen to be in the region G_- for the given n. Time t is in the units of ω_0^{-1}, which is of the order of nanoseconds.

and calculate the time dependent coefficients $\zeta_1(t)$, $\zeta_2(t)$, $\zeta_3(t)$ and $\zeta_4(t)$ satisfying the Schrödinger equation. Now, we can calculate the density matrix $\rho_{AB}(t) = |\psi(t)\rangle\langle\psi(t)|$ as

$$\rho_{AB}(t) = \begin{pmatrix} \rho_{11} & \rho_{12} & \rho_{13} & \rho_{14} \\ \rho_{21} & \rho_{22} & \rho_{23} & \rho_{24} \\ \rho_{31} & \rho_{32} & \rho_{33} & \rho_{34} \\ \rho_{41} & \rho_{42} & \rho_{43} & \rho_{44} \end{pmatrix}. \tag{2.44}$$

Here the matrix elements of $\rho_{AB}(t)$ are constructed through the coefficients $\rho_{nm} = \zeta_n \zeta_m^*$. The explicit expressions for the coefficients ζ_n are obtained by solving the Schrödinger equation and separating the equations for the coefficients is given in Appendix A . S-III .

For calculating the expectation values involving the spin part of the system we trace out the mathematical pendulum part A in the region G_-. The reduced density matrix of the

system is defined as $\hat{\rho}_B(t) = Tr_A(\hat{\rho})$ and given by

$$\begin{aligned}\hat{\rho}_B(t) &= \left(|\zeta_1|^2+|\zeta_3|^2\right)|0\rangle\langle 0| + \left(|\zeta_2|^2+|\zeta_4|^2\right)|1\rangle\langle 1| \\ &+ \left(\zeta_1\zeta_2^* + \zeta_3\zeta_4^*\right)|0\rangle\langle 1| + h.c..\end{aligned} \tag{2.45}$$

Let us calculate the expectation values of spin in the longitudinal and transverse directions defined earlier as $\langle\sigma_\alpha\rangle = Tr(\hat{\rho}_B\sigma_\alpha)$, $\alpha = x,y,z$.

$$\langle\sigma_z\rangle_{G_-} = |\zeta_1(t)|^2+|\zeta_3(t)|^2-|\zeta_2(t)|^2-|\zeta_4(t)|^2, \tag{2.46}$$

$$\langle\sigma_y\rangle_{G_-} = -2Im(\zeta_1(t)\zeta_2^*(t)+\zeta_3(t)\zeta_4^*(t)), \tag{2.47}$$

$$\langle\sigma_x\rangle_{G_-} = 2Re(\zeta_1(t)\zeta_2^*(t)+\zeta_3(t)\zeta_4^*(t)). \tag{2.48}$$

Fig. 2.4 indicates that the spin dynamics in the region G_- is similar to the spin dynamics in the region G_0. In the region G_0 both the longitudinal and the transverse spin components show larger amplitude of oscillation in the excited states, while in the region G_- the oscillation amplitudes of the longitudinal component $\langle\sigma_z(t)\rangle$ are smaller than in the G_0 region (see Fig. 2.4(c)). We see that c_1, d_1 and e_1 are negligibly small in comparison to b_1, therefore $\lambda_1^2 \approx \lambda_2^2 \approx b_1^2$. Taking this approximation into account, we can write $\langle\sigma_x\rangle_{G_-}$ in a simpler form as

$$\langle\sigma_x\rangle_{G_-} \approx 2(b_1e_1+c_1d_1)\frac{\sin^2\left(t\lambda_2\right)}{\lambda_2^2,}, \tag{2.49}$$

where the amplitude of oscillation is $\frac{2(b_1e_1+c_1d_1)}{\lambda_2^2}$ and frequency of oscillation is $\frac{\lambda_2}{\pi}$. In this region, there is a small variation of the amplitude and the frequency of oscillation with the quantum numbers n and l. Since G_- region is away from the line of separatrix, for a given

n, the amplitude of oscillations are linearly increasing (though small) and the frequency of oscillations are nearly constant with l. A similar description holds true for $\langle\sigma_y(t)\rangle_{G_-}$ and $\langle\sigma_z(t)\rangle_{G_-}$ cases.

2.5 Dissipation

In this section, we explore the decoherence processes. To keep a general discussion, we consider two different cases: First, the relaxation process will be described by the Markovian master equation. However, we note that the relaxation processes described by the Markovian master equation are not the only source of decoherence in NV centers. The other case which is the primary cause of decoherence for the NV centers usually is due the nuclear-spin bath surrounding the electron spin (see [121, 191] and references therein). At first, we consider the Markovian master equation that allows us to obtain an analytical result.

2.5.1 Markovian Lindblad master equation

To explore the decoherence due to the environment the Lindblad master equation approach is used. The Hamiltonian of the system is given by Eq. (2.17). Let us suppose the system time evolution is nonunitary but Markovian. The nonunitary evolution of the system may cause dissipation as the information may transmitted to the environment. The Liouville-von Neumann -Lindblad equation containing dissipation and decoherence terms describe this nonunitary Markovian evolution of the system. One can start with Liouville- von Neumann-Lindblad master equation for the density matrix [130, 192]

$$\frac{d\rho}{dt} = -i[H,\rho] + \gamma(\sigma_-\rho\sigma_+ - \frac{1}{2}(\sigma_+\sigma_-\rho + \rho\sigma_+\sigma_-)), \tag{2.50}$$

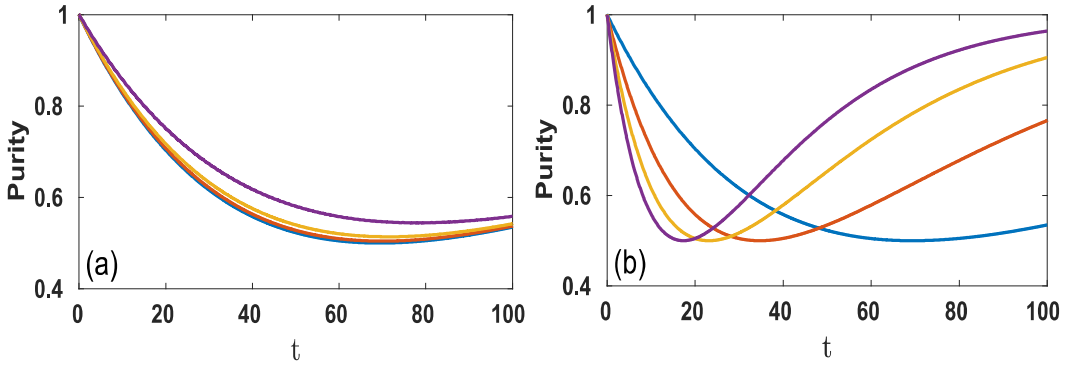

Fig. 2.5 Purity for the hybrid system of NV center and nonlinear oscillator. (a) Behavior of purity for a damping constant $\gamma = 0.01$ at an arbitrary interaction strength Q. The blue (solid), red (solid), yellow (solid) and purple (solid) lines represent $Q = 0.5$, $Q = 5$, $Q = 10$ and $Q = 25$ cases, respectively. (b) For an interaction strength $Q = 0.5$ but at arbitrary damping constant γ. The blue (solid), red (solid), yellow (solid) and purple (solid) lines represent $\gamma = 0.01$, $\gamma = 0.02$, $\gamma = 0.03$ and $\gamma = 0.04$ cases, respectively. In G_0 region for the quantum state $n = 4$. The barrier height $l = 10.785$ corresponds to the region G_0 in the vicinity of the transition into the region G_-. Time t is in the units of ω_0^{-1}, which is of the order of nanoseconds.

where γ is a dephasing parameter , and $\sigma_\pm = \sigma_x \pm i\sigma_y$ are dissipators. Let us consider the system in G_0 region. Then the differential equations for each element of the density matrix can be obtained from the Eq. (2.50) as

$$\begin{aligned}
\dot{\rho}_{11} &= -\gamma\rho_{11} + ic(\rho_{12} - \rho_{21}), \\
\dot{\rho}_{12} &= -\frac{\gamma}{2}\rho_{12} + i(-2b\rho_{12} + c(\rho_{11} - \rho_{22})), \\
\dot{\rho_{21}} &= -\frac{\gamma}{2}\rho_{21} + i(2b\rho_{21} + c(\rho_{22} - \rho_{11})), \\
\dot{\rho}_{22} &= \gamma\rho_{11} - ic(\rho_{12} - \rho_{21}).
\end{aligned} \tag{2.51}$$

The solution to the above four equations can be obtained by using the corresponding initial conditions $\rho_{11}(0) = 1$, $\rho_{12}(0) = 0$, $\rho_{21}(0) = 0$, $\rho_{22}(0) = 0$ has the form

$$\rho_{11}(t) = \frac{b^2 + c^2(\cos\sqrt{b^2 + c^2}t)^2}{(b^2 + c^2)} e^{-\gamma t}, \tag{2.52}$$

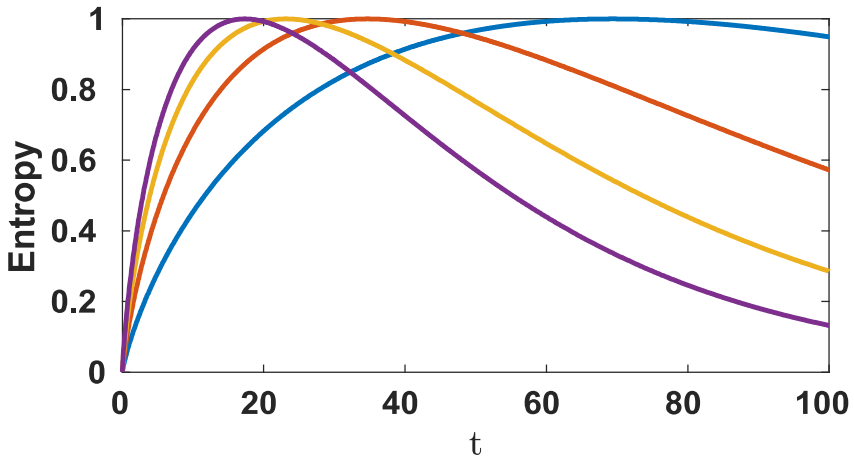

Fig. 2.6 Entropy of the hybrid system of NV center and nonlinear oscillator in the G_0 region for the quantum state $n = 4$. The barrier height $l = 10.785$ corresponds to the region G_0. The coupling strength $Q = 0.5$ at arbitrary damping constant γ. The blue (solid), red (solid), yellow (solid) and purple (solid) lines represent $\gamma = 0.01$, $\gamma = 0.02$, $\gamma = 0.03$ and $\gamma = 0.04$ cases, respectively. Time t is in the units of ω_0^{-1}, which is of the order of nanoseconds and entropy is in the unit of 'bits'.

$$\begin{aligned}\rho_{12}(t) &= \rho_{21}^{*}(t) \\ &= \frac{c(b - b\cos 2\sqrt{b^2+c^2}t - i\sqrt{b^2+c^2}\sin 2\sqrt{b^2+c^2}t)}{2(b^2+c^2)} e^{-\frac{\gamma}{2}t},\end{aligned} \tag{2.53}$$

$$\rho_{22}(t) = 1 + \left(\frac{c^2(\sin\sqrt{b^2+c^2}t)^2}{(b^2+c^2)} - 1\right)e^{-\gamma t}. \tag{2.54}$$

One can define the purity of the NV spin coupled to the mathematical pendulum and in contact with the environment as $\mathscr{P}(t,\rho) = Tr(\rho^2(t))$. $\mathscr{P}(t,\rho)$ is a quantifier of mixedness of the system. Using the expressions for the density matrix elements evolved in time in

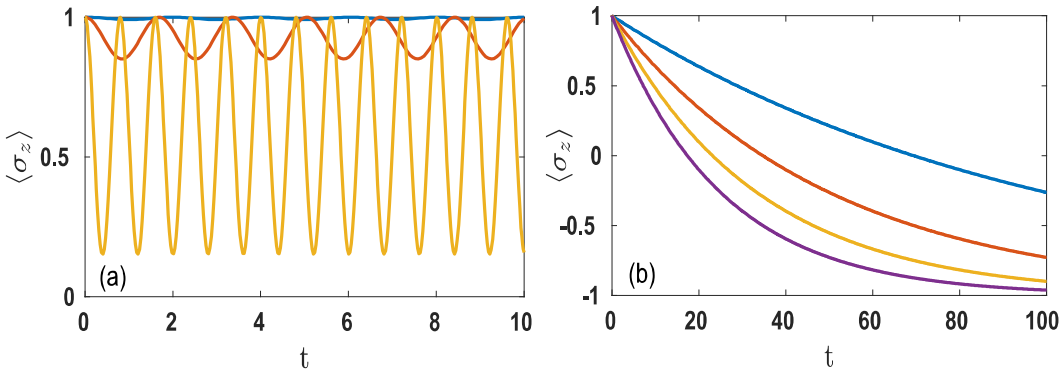

Fig. 2.7 Longitudinal spin component $\langle\sigma_z\rangle$ of the hybrid system of NV center and nonlinear oscillator (a). The blue (solid), red (solid) and yellow (solid) lines represent $Q=1$, $Q=5$ and $Q=25$ cases, respectively. For different damping coefficient γ and fixed coupling strength $Q=0.5$ (b). The blue (solid), red (solid), yellow (solid) and purple (solid) lines represent $\gamma=0.01$, $\gamma=0.02$, $\gamma=0.03$ and $\gamma=0.04$ cases, respectively. Both cases are in G_0 region for the quantum state $n=4$ is considered. The barrier height $l=10.785$ corresponds to the region G_0 in the vicinity of the transition to the G_- region. Time t is in the units of ω_0^{-1}, which is of the order of nanoseconds.

accordance with Eqs. (2.52)-(2.54), one can calculate $\mathscr{P}(t,\rho)$ as

$$\begin{aligned}\mathscr{P}(t,\rho) &= \big((8b^2\kappa^2+3c^4-(8b^2\kappa^2+3c^4)e^{\gamma t}+4\kappa^4e^{2\gamma t}+c^2(-1+e^{\gamma t})\\ &\quad (-4(b^2+\kappa^2)\cos 2\kappa t-c^2\cos 4\kappa t))/4\kappa^4\big)e^{-2\gamma t},\end{aligned} \tag{2.55}$$

where $\kappa^2=b^2+c^2$, b and c are defined in Eq. (2.23). It is obvious that the isolated system ($\gamma=0$) for any arbitrary coupling strength Q is always in a pure state. However, for nonzero γ, one can observe that for any arbitrary coupling strength Q, the system loses the purity as time goes on and evolves through the intermediate mixed state. Increasing the coupling strength enhances the purity, as seen in Fig. 2.5(a).

Fig. 2.5 (b) shows that the open quantum system for arbitrary γ initially prepared in the pure state evolves through the intermediate mixed state, dips down to 0.5 and finally reaches its value for the pure state. Interestingly, increasing the damping constants lowers the revival time of initial state. The quantum revival of the state is also reflected in the dynamics of von Neumann entropy of the system (see Fig. 2.6). For the pure state the von Neumann entropy $S=-\mathrm{Tr}(\rho\log_2\rho)$ is zero, and for the completely mixed state, S is

one. Fig.2.5 (b) and Fig. 2.6 show that for smaller damping coefficient, the system relaxes slowly and with more time needed for revival.

One can also analyze the dynamics of the longitudinal spin component $\langle\sigma_z\rangle$ as it is shown in Figs. 2.7(a) and 2.7(b). Fig. 2.7(a) shows that the amplitude of the oscillation increases with increasing the coupling constant Q. Also, faster switching of the longitudinal spin component can be seen while increasing Q. For fixed coupling constant $\langle\sigma_z\rangle$ does not oscillates but decays. Increasing the damping coefficient increases the decay rate (see Fig. 2.7(b)).

As we see, the master equation has a single steady state which is a pure state. Therefore, the dynamics asymptotically converges to a pure state.

2.5.2 Fluctuations due to the spin bath

The hyperfine coupling of the NV spin to the ^{13}C nuclear spins causes a dephasing of the NV spin. This effect can be described by considering N independent reservoirs coupled to the NV spin. It has been shown that the dynamics of the spin in the presence of the N reservoirs can be Markovian or non-Markovian[130, 193, 194] depending upon the the number of reservoirs. If the number of reservoirs are above the cut off N_c, then the reservoirs act as a non-Markovian channel. N_c depends on the bath parameters and the coupling between NV spin and reservoirs. Let us consider the system in G_0 region is coupled to N independent bosonic reservoirs of field modes initially in the vacuum.[195, 196, 197] The Hamiltonian of the system and the reservoir is given as

$$\hat{H} = \hat{H}_{eff} + \sum_{n=1}^{N}\sum_{k}[\omega_{n,k}\hat{a}^{\dagger}_{n,k}\hat{a}_{n,k} + g_{n,k}(\hat{a}^{\dagger}_{n,k}\hat{\sigma}^{-} + \hat{a}_{n,k}\hat{\sigma}^{+}], \tag{2.56}$$

where $\hat{H}_{eff} = a\mathscr{I} - \sqrt{b^2+c^2}\hat{\sigma}^z$, $\mathscr{I}$ is the identity matrix, and the coefficients a, b and c in $\hat{H}_{eff}$, are given in Eq.(2.23). In what follows we neglect the constant term and retain only the part involved in the spin dynamics $\hat{H}_{eff} = -\omega_{eff}\hat{\sigma}^z$, where $\omega_{eff} = \sqrt{b^2+c^2}$.

The operator $\hat{a}_{n,k}$ ($\hat{a}^{\dagger}_{n,k}$) in Eq.(2.56) is annihilation (creation) operator of the k^{th} bosonic field mode of the n^{th} reservoir.

Let us consider the initial state of the system in a general form

$$|\psi(0)\rangle = c_0(0)|0\rangle + c_1(0)|1\rangle, \tag{2.57}$$

where $c_0(0)$ and $c_1(0)$ are coefficients at $t = 0$. The state of reservoirs is of the form $\prod_{n=1}^{N} |\bar{0}\rangle_{n,r}$ with $|\bar{0}\rangle_{n,r} = \prod_{k=1} |0_k\rangle_{n,r}$. Then the joint state of the system and the reservoir is given by $|\Psi(0)\rangle = |\psi(0)\rangle \otimes \prod_{n=1}^{N} |\bar{0}\rangle_{n,r}$ which after evolution becomes

$$|\Psi(t)\rangle \quad = \quad [c_0(0)|0\rangle + c_1(t)|1\rangle] \otimes \prod_{n=1}^{N} |\bar{0}\rangle_{n,r} + |0\rangle \otimes \sum_{n=1}^{N} \sum_{k} c_{n,k}(t)|1_k\rangle_{n,r}. \tag{2.58}$$

In the above equation $c_1(t)$ and $c_{n,k}$ are time dependent coefficients of the spin system and the reservoir, respectively. Using Schrodinger's equation Eq.(2.33), we obtain the time dependent coefficients in the interaction picture which are governed by the differential equations [196]:

$$\frac{d}{dt}c_1(t) = -i \sum_{n=1}^{N} \sum_{k} h_{n,k} e^{i(w_{eff} - w_{n,k})t} c_{n,k}(t), \tag{2.59}$$

$$\frac{d}{dt}c_{n,k}(t) = -i h^{*}_{n,k} e^{-i(w_{eff} - w_{n,k})t} c_1(t). \tag{2.60}$$

We observe that the summation $\sum_k |h_{n,k}|^2 e^{i(w_{eff} - w_{n,k})t}$ appearing in the above equation is the correlation function $s_n(t)$ of the n^{th} reservoir. In the limit of a large number of modes, the summation can be obtained in the form of integration in term of spectral density $j_n(\omega)$ as

$$s_n(t - t_1) = \int d\omega\, j_n(\omega) \exp[i(\omega_{eff} - \omega)(t - t_1)]. \tag{2.61}$$

The coefficient $c_1(t)$ can now be expressed as

$$\frac{d}{dt}c_1(t) = -\int_0^t dt_1 c_1(t_1) S(t-t_1), \tag{2.62}$$

with $S(t-t_1) = \sum_{n=1}^{N} s_n(t-t_1)$ and the spectral density $j_n(\omega)$ is assumed to be Lorentzian form $j_n(\omega) = g_n\tau_n^2/\big(2\pi[(\omega_{eff}-\omega-\delta_n)^2+\tau_n^2]\big)$,[130, 197] where g_n is the system-reservoir coupling strength and τ_n^{-1} is the correlation time of the reservoir. The central frequency of the n^{th} reservoir ω_n^c is detuned by δ_n from the ω_{eff}. Considering a simpler case of identical reservoirs and defining $g_n/\tau_n = g/\tau$, $\omega_n^c = \omega^c$ and $\delta_n = \delta$, we can obtain the function $c_1(t)$ in a compact form as

$$c_1(t) = c_1(0)e^{-\frac{(\tau-i\delta)t}{2}}\left[\cosh\left(\frac{\kappa_x t}{2}\right) + \frac{(\tau-i\delta)}{\kappa_x}\sinh\left(\frac{\kappa_x t}{2}\right)\right], \tag{2.63}$$

with $\kappa_x = \sqrt{(\tau-i\delta)^2 - 2Ng\tau}$ and $\delta = \omega_{eff} - \omega^c$. We observe that the amplitude of $c_1(t)$ is decaying with a rate τ^{-1} and oscillating with frequency δ. We can write the dynamics of the NV spin in terms of a reduced density matrix in the basis of $|0\rangle$ and $|1\rangle$ by tracing out the reservoirs as shown in Appendix A . S-V,[130]

$$\rho_s(t) = \begin{pmatrix} 1-|c_1(t)|^2 & c_0(0)c_1^*(t) \\ c_0^*(0)c_1(t) & |c_1(t)|^2 \end{pmatrix}, \tag{2.64}$$

where

$$\begin{aligned} |c_1(t)|^2 &= |c_1(0)|^2 e^{-\tau t}\Big[\Big(\cosh\Big(\frac{\kappa' t}{2}\Big)\cos\Big(\frac{\kappa'' t}{2}\Big) + \frac{\kappa_1}{|\kappa_x|^2}\sinh\Big(\frac{\kappa' t}{2}\Big)\cos\Big(\frac{\kappa'' t}{2}\Big) \\ &- \frac{\kappa_2}{|\kappa_x|^2}\cosh\Big(\frac{\kappa' t}{2}\Big)\sin\Big(\frac{\kappa'' t}{2}\Big)\Big)^2 + \Big(\sinh\Big(\frac{\kappa' t}{2}\Big)\sin\Big(\frac{\kappa'' t}{2}\Big) \\ &+ \frac{\kappa_1}{|\kappa_x|^2}\cosh\Big(\frac{\kappa' t}{2}\Big)\sin\Big(\frac{\kappa'' t}{2}\Big) + \frac{\kappa_2}{|\kappa_x|^2}\sinh\Big(\frac{\kappa' t}{2}\Big)\cos\Big(\frac{\kappa'' t}{2}\Big)\Big)^2\Big] \end{aligned} \tag{2.65}$$

and κ' (κ'') are real (imaginary) part of κ_x and $\kappa_1 = (\tau\kappa' + \delta\kappa'')$, $\kappa_2 = (\delta\kappa' - \tau\kappa'')$.

In order to ensure that the set of parameters lead us to the dynamics of the system in non-Markovian regime we calculate the trace distance $\mathscr{D}(\rho_1(t), \rho_2(t))$ between the time evolved states of any two quantum states $\rho_1(t)$ and $\rho_2(t)$ of the system and find the rate of change of the trace distance $F(N,t)$. For all the Markovian processes $F(N,t)$ is less than or equal to zero which means that the information will always flow from the system to the environment. However, if there exist a pair of initial states for which $F(N,t)$ is positive even for a certain time, the process is said to be non-Markovian. All those times when $F(N,t)$ is positive, the distinguishability of the time evolved pair of initial states increases resulting a back flow of information from the environment to the system. It has been shown [198] that if we start with a pair of initial states $|\psi_{1,2}(0)\rangle = \frac{1}{\sqrt{2}}(|0\rangle \pm |1\rangle)$, the trace distance comes out to be $|c_1(t)|$ and the rate of change of the trace distance turns out to be

$$F(N,t) = \frac{d|c_1(t)|}{dt}. \tag{2.66}$$

The full expression of $F(N,t)$ is shown in Appendix A . S-IV. If $F(N,t)$ is larger than zero in a certain time interval, the reservoir displays a non-Markovian behavior [194].

This fact gives a criteria for the choice of parameters τ, g, δ and N such that the reservoirs act as a non-Markovian channel. We can define the quantity $[\tau/2g + 1] = N_c$ when $\delta = 0$. For instance, $g = \frac{3\tau}{8}$ gives $N_c = 2$. It is worth to note that away from the resonance *i.e.*, $\delta \neq 0$, the above definition of N_c will not hold. For example, for $\delta = 0.2g$, the critical number of reservoirs $N_c = 3$ and for $\delta = 0.5g$, the critical number of reservoirs becomes $N_c = 4$ for the same choice of $\tau/2g$. In Fig. 2.8 we have shown a contour plot of $F(N,t)$ with N and t for parameters $\delta = 0.2g$ and $g = \frac{3\tau}{8}$. The $F(N,t) > 0$ regions form a comb like contours. We see that the amplitude of oscillations of $F(N,t)$ increases with increasing N and regions of prominent $F(N,t) < 0$ and $F(N,t) > 0$ are visible for high N.

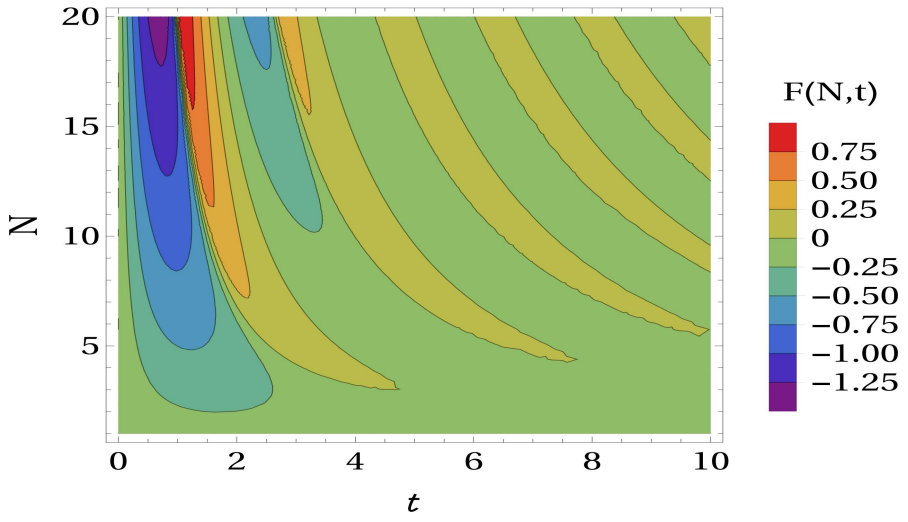

Fig. 2.8 $F(N,t)$ is plotted for different values of number of reservoirs N and time t. Weak system-reservoir coupling is considered with parameters $\tau = 1$, $g = \frac{3\tau}{8}$ and $\delta = 0.2$. Time t is in the units of ω_0^{-1}, which is of the order of nanoseconds.

We can calculate the purity of the NV spin using $\mathscr{P} = Tr(\rho_s^2(t))$ and get

$$\mathscr{P} = 1+2|c_1(t)|^2\Big(|c_1(t)|^2+|c_0(0)|^2-1\Big). \tag{2.67}$$

We can see from Fig. 2.9 that the system loses the purity as time progresses while evolving through the intermediate mixed state, and finally reaching to a pure state. We see that increasing the number of reservoirs leads to a quicker revival of the pure state and when system-reservoir coupling is not present *i.e.*, $\tau = 0$, the system remains in the pure state. The oscillations in the purity is due to the δ term in the expression of $c_1(t)$. For the weak system-reservoir coupling *i.e.*, $g = \frac{3\tau}{8}$ and $\delta = 0.2g$ the system shows Markovian dynamics for $N = 2$. In this case if we add more reservoirs the system will show non-Markovian behaviour. In our case we have used the parameters $\tau = 1$, $g = 3\tau/8$ and $\delta = 0.2$ (solid) corresponds to $\delta < g/\tau$, $\delta = 0.5$ (dotted) corresponds to $\delta > g/\tau$. Increasing the detuning parameter δ ($\geq g/\tau$) increases the number of reservoirs and enhances the back flow of the information from the environment to the system. [194, 195, 199]

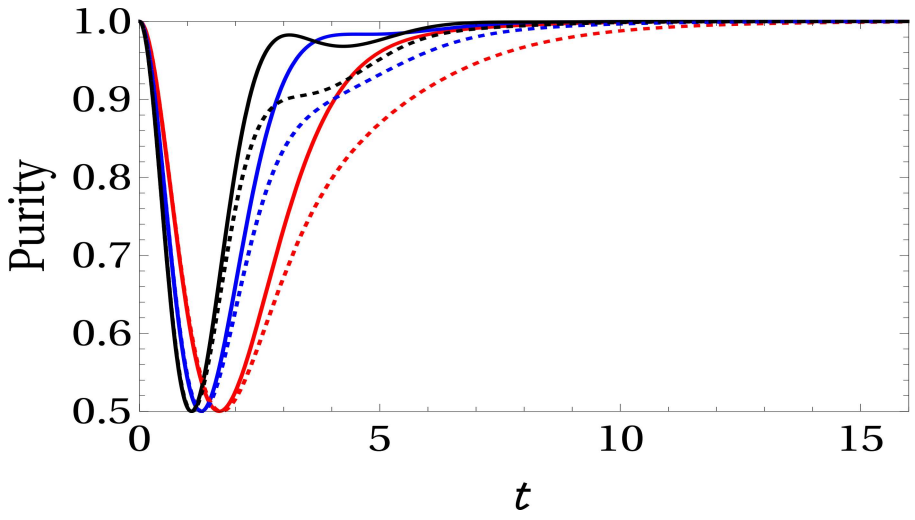

Fig. 2.9 Purity of the system coupled with N reservoirs within a weak coupling regime with parameters $\tau = 1$ and $g = \frac{3\tau}{8}$, $\delta = 0.2$ (solid), $\delta = 0.5$ (dotted) for $c_0(0) = 0$ and $c_1(0) = 1$. The red, blue and black lines represent $N = 2,3,4$ cases, respectively. Time t is in the units of ω_0^{-1}, which is of the order of nanoseconds.

2.6 Multilevel dynamics

The presence of the spin-oscillator coupling term leads to mixing of the nonlinear oscillator states. We assume that initially the system is in the G_0 region. Energy spectrum of the system is such [187, 188, 189], that for a given value of the barrier height l, only several energy levels $E_n(l)$ and states belong to the region G_0. We assume that these two states are neighboring states ce_n, se_{n+1}. Then the computational basis vectors are: $|ce_n(\varphi,l)\rangle \otimes |0\rangle$, $|ce_n(\varphi,l)\rangle \otimes |1\rangle$, $|se_{n+1}(\varphi,l)\rangle \otimes |0\rangle$, and $|se_{n+1}(\varphi,l)\rangle \otimes |1\rangle$. The Hamiltonian of the system is

$$\hat{H} = \begin{pmatrix} a_2+b_2 & c_2 & d_2 & e_2 \\ c_2 & a_2-b_2 & e_2 & -d_2 \\ d_2 & e_2 & f_2+g_2 & h_2 \\ e_2 & -d_2 & h_2 & f_2-g_2 \end{pmatrix}, \tag{2.68}$$

where $a_2 = a_n(l)$, $b_2 = \frac{\omega_0}{2} + \frac{1}{2}Qr_2\cos\alpha$, $c_2 = \frac{1}{2}Qr_2\sin\alpha$, $d_2 = \frac{1}{2}Qs_2\cos\alpha$, $e_2 = \frac{1}{2}Qs_2\sin\alpha$, $f_2 = b_{n+1}(l)$,$g_2 = \frac{\omega_0}{2} + \frac{1}{2}Qt_2\cos\alpha$, $h_2 = \frac{1}{2}Qt_2\sin\alpha$,

$$r_2 = [\{\frac{\pi}{2}\left(A_1^{(2n+1)}(l)\right)^2 + \pi\sum_{r=0}^{\infty} A_{2r+1}^{(2n+1)}(l)A_{2r+3}^{(2n+1)}(l)\}], \tag{2.69}$$

$$t_2 \;=\; [\{\frac{\pi}{2}\left(-B_1^{(2n+1)}(l)\right)^2 + \pi\sum_{r=0}^{\infty} B_{2r+1}^{(2n+1)}(l)B_{2r+3}^{(2n+1)}(l)\}], \tag{2.70}$$

$s_2 = \langle ce_n(\varphi,l)|\cos(2\varphi)|se_{n+1}(\varphi,l)\rangle$.

The multilevel dynamics of the system in the subgroup G_0 is far more complicated. Let us define the initial state of the system in G_0 region as

$$|\psi(0)\rangle = |ce_n(\varphi,l)\rangle \otimes |0\rangle. \tag{2.71}$$

We use the following ansatz for the wave function in the region G_0:

$$\begin{aligned}|\psi(t)\rangle &= S_1(t)|ce_n(\varphi,l)\rangle|0\rangle + S_2(t)|ce_n(\varphi,l)\rangle|1\rangle + \\ &S_3(t)|se_{n+1}(\varphi,l)\rangle|0\rangle + S_4(t)|se_{n+1}(\varphi,l)\rangle|1\rangle.\end{aligned} \tag{2.72}$$

and solve the Schrödinger equation (Eq. (2.33)) for the Hamiltonian Eq. (2.68) to get coefficients $S_1(t)$, $S_2(t)$, $S_3(t)$ and $S_4(t)$. Using this solution $\psi(t)$ we calculate the density matrix $\rho_{AB}(t) = |\psi(t)\rangle\langle\psi(t)|$ which is given as

$$\rho_{AB}(t) = \begin{pmatrix} \rho_{11} & \rho_{12} & \rho_{13} & \rho_{14} \\ \rho_{21} & \rho_{22} & \rho_{23} & \rho_{24} \\ \rho_{31} & \rho_{32} & \rho_{33} & \rho_{34} \\ \rho_{41} & \rho_{42} & \rho_{43} & \rho_{44} \end{pmatrix}. \tag{2.73}$$

We trace out partially the mathematical pendulum part and calculate the reduced density matrix $\hat{\rho}_B(t)$ of the spin part of the system in the region G_0 as

$$\begin{aligned}\hat{\rho}_B(t) &= \left(|S_1|^2+|S_3|^2\right)|0\rangle\langle 0| + \left(|S_2|^2+|S_4|^2\right)|1\rangle\langle 1| \\ &+ \left(S_1S_2^*+S_3S_4^*\right)|0\rangle\langle 1| + h.c., \end{aligned} \tag{2.74}$$

The expectation values of longitudinal spin component $\langle\sigma_z\rangle$ and transverse spin components $\langle\sigma_x\rangle$, $\langle\sigma_y\rangle$ are given as

$$\langle\sigma_z\rangle = |S_1(t)|^2+|S_3(t)|^2-|S_2(t)|^2-|S_4(t)|^2, \tag{2.75}$$

$$\langle\sigma_y\rangle = -2Im(S_1(t)S_2^*(t)+S_3(t)S_4^*(t)), \tag{2.76}$$

and

$$\langle\sigma_x\rangle = 2Re(S_1(t)S_2^*(t)+S_3(t)S_4^*(t)). \tag{2.77}$$

The state given by Eq. (2.74) is a multilevel product state as the eigenvalues of the reduced density matrix are $\rho_{11}^B = |\alpha|^2+|\beta|^2$, $\rho_{22}^B = 0$ and von Neumann entropy $\mathrm{Tr}\rho_B\log_2\rho_B$ is zero. The results obtained for the spin dynamics for the multilevel case are shown in the Fig. 2.10 (a), (b) and (c). The transverse spin components $\langle\sigma_x\rangle$, $\langle\sigma_y\rangle$ indicate switching and the amplitude of the oscillation increases with increase in the quantum number n. In Fig. 2.10 (a) and (b) the behaviour of $\langle\sigma_x\rangle$, $\langle\sigma_y\rangle$ is the same as that of the Fig. 2.2 (a) and (b) due to a large energy gap between the mathematical pendulum states considered for given n and l. The longitudinal spin part $\langle\sigma_z\rangle$ decays and more prominent so for certain value of n. For instance, in Fig. 2.10 (c), $n = 3$ and $l = 7.535$ decay due to transition between neighboring states is observed. For this case, we know that initially $|S_1(t)|^2$ is one and all other probabilities are zero. We can show numerically that as time

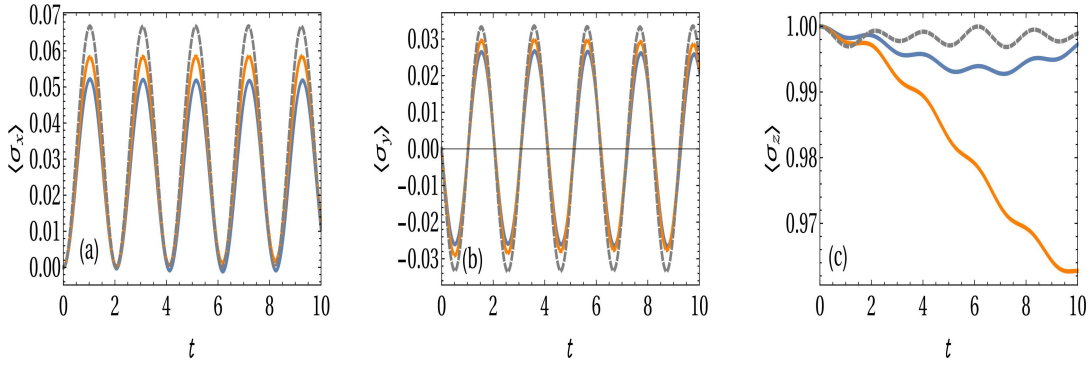

Fig. 2.10 (a) Transverse spin component $\langle\sigma_x\rangle$, (b) transverse spin component $\langle\sigma_y\rangle$, and (c) longitudinal spin component $\langle\sigma_z\rangle$ plotted as function of time for the bipartite system $\hat{\rho}_{AB}$ in the region G_0 for different multilevel quantum states $n = 2,3,4$. The blue (solid), orange (solid) and violet (dashed) lines represent $n = 2, l = 3.855$, $n = 3, l = 7.535$ and $n = 4, l = 10.785$ cases, respectively. The values of barrier heights l are chosen to be in the region G_0 in the vicinity to the transition into the region G_-. The interaction strength between nonlinear oscillator and NV spin is $Q = 0.5$. Time t is in the units of ω_0^{-1}, which is of the order of nanoseconds.

progresses $|S_1(t)|^2$ decreases and $|S_4(t)|^2$ increases, while $|S_2(t)|^2$ and $|S_3(t)|^2$ are showing a small variation. This indicates a major transition from the initial state $|ce_n(\varphi,l)\rangle|0\rangle$ to the neighbouring state $|se_{n+1}(\varphi,l)\rangle|1\rangle$.

We note that by steering parameters of the driving term in Eq.(2.3), we can easily achieve the desired value of l from the region G_0 and switch the NV spin from $|0\rangle$ state to $|1\rangle$.

2.7 Unitary generation of coherence

The advantage of NV centers over other qubit systems is their relatively low decoherence rate. On the long run, even a slow decoherence leads to substantial effects on the dynamics of the system. Due to decoherence the off-diagonal elements of the density matrix diminish. The question now is whether this system can evolve to some other state with finite off-diagonal elements signaling coherence, a mechanism that may be useful for some coherence-based operations [200, 201, 202, 203]. The mixedness of the state

ρ is characterized by the linear entropy given as $[1-Tr(\rho^2)]$. Under unitary evolution the mixedness never changes. It will be important to see whether the coherence can be generated under the unitary evolution. Suppose that the system is prepared in a mixed state $\hat{\rho}(0)$ initially corresponding to the Hamiltonian $\hat{H}_0$. We consider the unitary evolution of the state $\hat{\rho}(0)$ governed by the operator $\hat{U} = \left(\exp\left(-\frac{i}{\hbar}\int \hat{H}dt\right)\right)$, where $\hat{H} = \hat{H}_0 + \hat{V}$. For obtaining closed analytical result, in what follows, we consider a sudden quench of the Zeeman splitting $\frac{1}{2}\Delta\omega_0$, *i.e.*, $(\omega_0, t<0) \rightarrow (\omega_0+\Delta\omega_0, t>0)$. Let us begin by assuming the system to be initially in the region G_0 and prepared in the mixed state as:

$$\hat{\rho}(0) = p_1|\phi_1\rangle\langle\phi_1| + p_2|\phi_2\rangle\langle\phi_2|. \tag{2.78}$$

Where $|\phi_1\rangle$ and $|\phi_2\rangle$ are the eigenstates of Hamiltonian in G_0 region. Following the idea put forward in Refs.[204, 205], we present the total Hamiltonian Eq. (2.17) after the quench in the form:

$$\hat{H} = \hat{H}_0 + \hat{V}, \tag{2.79}$$

where,

$$\begin{aligned} \hat{H}_0 &= \hat{H}_m + \hat{H}_s + Q\cos(\varphi)\hat{S}_z \\ \hat{V} &= \frac{1}{2}\Delta\omega_0\sigma_z. \end{aligned} \tag{2.80}$$

We note that $\hat{S}_z$ contains the raising and lowering operators $\hat{\sigma}_+$, $\hat{\sigma}_-$ and therefore the commutator is not zero $[\hat{H}_s, \hat{V}] \neq 0$. We exploit the relative entropy as an entropic measure for coherence:

$$\mathscr{C}\left(\hat{\rho}(t)|\hat{\rho}_d\right) = Tr\{\hat{\rho}(t)\ln\hat{\rho}(t) - \hat{\rho}(t)\ln\hat{\rho}_d\}. \tag{2.81}$$

Here $\hat{\rho}_d$ is the diagonal part of the propagated density matrix $\hat{\rho}(t) = \exp(\frac{i}{\hbar}\hat{H}t)\hat{\rho}(0)\exp(-\frac{i}{\hbar}\hat{H}t)$. The larger is the departure from the $\hat{\rho}_d$, larger is the relative entropy $\mathscr{C}\left(\hat{\rho}(t)|\hat{\rho}_d\right)$. This departure from the $\hat{\rho}_d$ is quantified by the non-zero off-diagonal part of $\hat{\rho}(t)$. Since we start from an incoherent state $\hat{\rho}(0)$, the non zero off-diagonal elements of $\hat{\rho}(t)$ signal the generation of coherence.

As for the relation between coherence and purity we refer to Ref. [206] and Ref. [207] stating

$$\mathscr{C}\left(\hat{\rho}(t)|\hat{\rho}_d\right) \leq \sqrt{2\mathscr{P}-1}. \tag{2.82}$$

Eq.(2.82) shows that there is an upper bound of the coherence quantified through the purity $\mathscr{P}$. This means that during the unitary evolution, coherence can be changed even though purity is invariant under unitary evolution $\mathscr{P}(\hat{\rho}(t)) = \mathscr{P}(\hat{\rho}(0))$. For incoherent unitaries coherence is constant [208]. The time evolved state $\rho(t)$ for the initial state given by Eq. (2.78) and the Hamiltonian given by Eq. (2.79) is calculated as

$$\begin{aligned}
\hat{\rho}(t) &= \left(p_1|\langle\psi_1|\phi_1\rangle|^2 + p_2|\langle\psi_1|\phi_2\rangle|^2\right)|\psi_1\rangle\langle\psi_1| + \left(p_1|\langle\psi_2|\phi_1\rangle|^2 + p_2|\langle\psi_2|\phi_2\rangle|^2\right)|\psi_2\rangle\langle\psi_2| \\
&+ \exp\left(-\frac{i}{\hbar}(E_1-E_2)t\right)\left(p_1\langle\phi_1|\psi_2\rangle\langle\psi_1|\phi_1\rangle + p_2\langle\phi_2|\psi_2\rangle\langle\psi_1|\phi_2\rangle\right)|\psi_1\rangle\langle\psi_2| \\
&+ \exp\left(\frac{i}{\hbar}(E_1-E_2)t\right)\left(p_1\langle\phi_1|\psi_1\rangle\langle\psi_2|\phi_1\rangle + p_2\langle\phi_2|\psi_1\rangle\langle\psi_2|\phi_2\rangle\right)|\psi_2\rangle\langle\psi_1|.
\end{aligned} \tag{2.83}$$

Here $|\phi_{1,2}\rangle$ are the eigenvectors and $E_{1,n}(l), E_{2,n}(l)$ are the eigenvalues of $\hat{H}_0(l)$ given in the explicit form as

$$
\begin{aligned}
&|\phi_1\rangle = |ce_n(l)\rangle \otimes (\alpha_1|1\rangle + \beta_1|0\rangle)\,,\\
&|\phi_2\rangle = |ce_n(l)\rangle \otimes (\beta_1|1\rangle - \alpha_1|0\rangle)\,,\\
&\alpha_1 = 1/\sqrt{\lambda^2+1},\ \beta_1 = \lambda/\sqrt{\lambda^2+1},\\
&\lambda = (b+\sqrt{b^2+c^2})/c,\\
&E_{1,n}(l) = a+\sqrt{b^2+c^2}, E_{2,n}(l) = a-\sqrt{b^2+c^2},
\end{aligned}
\tag{2.84}
$$

and coefficients a, b and c are already defined in section IV. We write the Hamiltonian after the quench $\hat{H}$ in the diagonal basis of H_0 as

$$
\hat{H} = \begin{pmatrix} E_{1,n}(l)+J & Y \\ Y & E_{2,n}(l)-J) \end{pmatrix}, \tag{2.85}
$$

where J and Y are given as:

$$
\begin{aligned}
&J = -\Delta\omega_0(\alpha_1^2-\beta_1^2),\\
&Y = -2\Delta\omega_0\alpha_1\beta_1.
\end{aligned}
\tag{2.86}
$$

The eigenvectors of $\hat{H}$ take explicit form as:

$$
\begin{aligned}
&|\psi_1\rangle = \zeta_1|\phi_1\rangle + \zeta_2|\phi_2\rangle,\\
&|\psi_2\rangle = \zeta_2|\phi_1\rangle - \zeta_1|\phi_2\rangle.
\end{aligned}
\tag{2.87}
$$

The coefficients ζ_1, ζ_2, eigenvalues of $\hat{H}$ and the rest of the information are presented in the Appendix A . S-VI. Taking into account Eq.(2.83)-Eq.(2.87) we rewrite the propagated density matrix in the more compact form

$$\hat{\rho}(t) = (p_1\zeta_1^2 + p_2\zeta_2^2)|\psi_1\rangle\langle\psi_1| + (p_1\zeta_2^2 + p_2\zeta_1^2)|\psi_2\rangle\langle\psi_2|$$
$$+\exp(-i\omega_{12}t)\zeta_1\zeta_2(p_1 - p_2)|\psi_1\rangle\langle\psi_2| + \exp(i\omega_{12}t)\zeta_1\zeta_2(p_1 - p_2)|\psi_2\rangle\langle\psi_1|. \tag{2.88}$$

Note that the evolved density matrix $\hat{\rho}(t)$, Eq.(2.88) is not diagonal in the basis Eq.(2.87) of the quenched Hamiltonian Eq. (2.85). Diagonalizing the evolved density matrix $\hat{\rho}(t)$ (Eq.(2.88)) we obtain the following eigenvectors

$$|\rho_1\rangle = \nu_1|\psi_1\rangle + \nu_2|\psi_2\rangle,$$
$$|\rho_2\rangle = \nu_2|\psi_1\rangle - \nu_1|\psi_2\rangle. \tag{2.89}$$

The coefficients ν_1, ν_2 and eigenvalues are presented in the Appendix A . S-VI. Taking into account Eq.(2.83)-Eq.(2.89), for the quantum coherence Eq.(2.81) we derive

$$\begin{aligned}\mathscr{C}\left(\hat{\rho}(t)|\hat{\rho}_d\right) &= p_1\ln(p_1) + p_2\ln(p_2) - p_1|\langle\rho_1|\psi_1\rangle|^2\ln(p_1\zeta_1^2 + p_2\zeta_2^2)\\ &- p_2|\langle\rho_2|\psi_2\rangle|^2\ln(p_1\zeta_2^2 + p_2\zeta_1^2) - p_1|\langle\rho_1|\psi_2\rangle|^2\ln(p_1\zeta_2^2 + p_2\zeta_1^2)\\ &- p_2|\langle\rho_2|\psi_1\rangle|^2\ln(p_1\zeta_1^2 + p_2\zeta_2^2),\end{aligned} \tag{2.90}$$

or after using trigonometric parametrization (see Appendix A . S-VI) in the explicit form:

$$\begin{aligned}\mathscr{C}\left(\hat{\rho}(t)|\hat{\rho}_d\right) &= p_1\ln(p_1) + p_2\ln(p_2)\\ &- \left(p_1\sin^2\Theta + p_2\cos^2\Theta\right)\ln\left(p_1\sin^2\Theta + p_2\cos^2\Theta\right)\\ &- \left(p_1\cos^2\Theta + p_2\sin^2\Theta\right)\ln\left(p_1\cos^2\Theta + p_2\sin^2\Theta\right).\end{aligned} \tag{2.91}$$

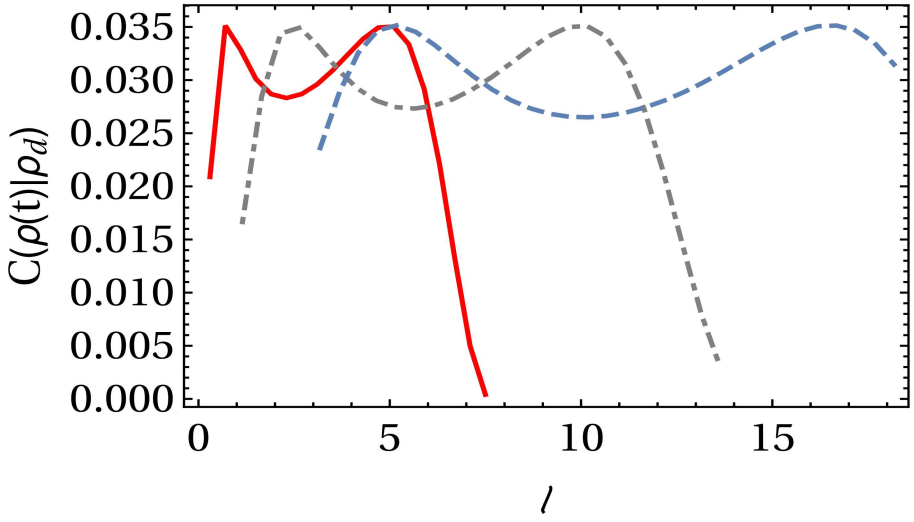

Fig. 2.11 The Coherence $\mathscr{C}(\rho(t)|\rho_d)$ plotted for the bipartite system in the region G_0 for different quantum states $n = 2,3,4$ and corresponding barrier height l in G_0 region . The red (solid), violet (Dotted-Dashed) and blue (Dashed) lines represent $n = 2$, $n = 3$ and $n = 4$ cases, respectively. The parameter used for the plot is $p_1 = 0.9$ and $p_2 = 0.1$, $\Delta\omega_0 = 0.8$ and $\omega_0 = 1$, $Q = 5$. Barrier height l is in units of $\frac{U}{\omega'}$.

All the parameters from Eq.(2.91) in the explicit form are presented in the Appendix A . S-VI. The hallmark of quantum chaos is the enhanced fluctuations which is inherent in this system, for more details see Ref. [189]. Therefore, the coherence $\mathscr{C}\left(\hat{\rho}(t)|\hat{\rho}_d\right)$ is rather sensitive with respect to the initial state and values of the parameters. Further, it is worth noting that the dynamical chaos emerges in the vicinity of the classical separatrix. In the quantum case, this region corresponds to crossover region between G_0 and G_-. In particular, this corresponds to the selective choice of the barrier height for each quantum state, *i.e.*, $(n = 2, l = 0.3 - 7.51)$, $(n = 3, l = 1.15 - 13.93)$, and $(n = 4, l = 3.18 - 18.4)$. We plot the coherence from Eq.(2.91) as a function of the barrier height l as shown in Fig. 2.11. As we see the generation of coherence is maximal when l is chosen from the chaotic region.

The result can be explained as follows: the analytical solution of the classical mathematical pendulum Eq.(2.18) has a bifurcation features:

$$\triangle I_+ = \sqrt{(E+U)/\omega'}\, dn\left[\omega'\sqrt{(E+U)/\omega'}t, k\right], \tag{2.92}$$

for $E > U$ and

$$\triangle I_{-} = \sqrt{(E+U)/\omega'}cn\left[\omega'\sqrt{(E+U)/\omega'}t, 1/k\right], \tag{2.93}$$

for $E < U$. Here $cn(\cdots)$, $dn(\cdots)$ are Jacobi elliptic functions and parameter is defined as follows $k = \sqrt{2U/(E+U)}$. When $k \to 1$ in the system occurs bifurcation and solutions take a form of instanton:

$$\Delta I_{+} = I_{-} = \frac{\sqrt{2U/\omega'}}{\cosh(\sqrt{2U\omega'}t)}. \tag{2.94}$$

Any small perturbation applied to the system in the vicinity of the bifurcation region $k \to 1$ leads to the formation of dynamical chaos and homoclinic tangle. [186] The width of the homoclinic tangle read:

$$\frac{|E - U/\omega'|}{U} \preceq \exp\left(-\pi\frac{\nu\sqrt{\omega'}}{\sqrt{U}}\right). \tag{2.95}$$

Phase trajectories of the system passing through the homoclinic tangle have limited memory, meaning that the information about the initial conditions is gradually lost. By analogy with the classical case, we presume that the quantum systems evolved through the region of quantum chaos have limited memory and weakly depend on the initial state. If we consider a maximally mixed state (infinite temperature state), we would not worry about the initial state preparation. Quantum chaos can sustain the generation of coherence from the mixed initial state. We aim to explore the signature of the quantum chaos and define quantum rescaled distance from the homoclinic tangle for the odd states $n' = 2n+1$

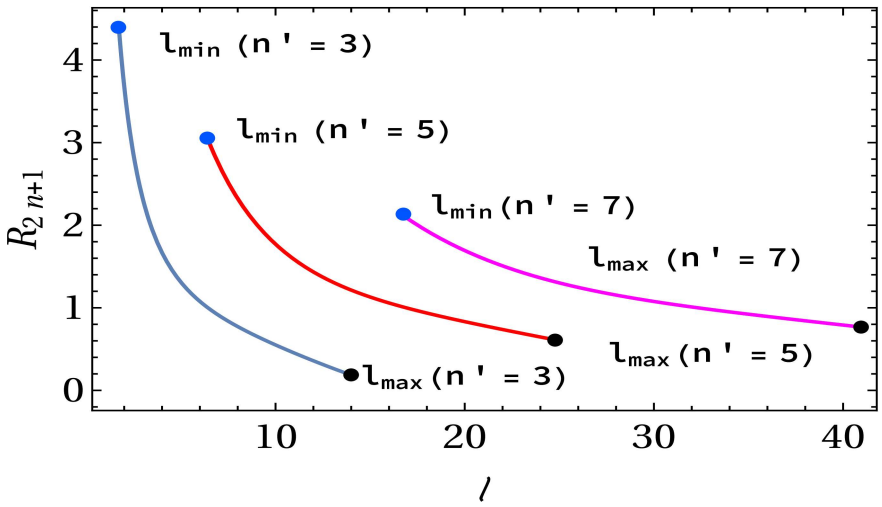

Fig. 2.12 The quantum distance R_{2n+1} from the classically chaotic region plotted as a function of the barrier height l. The values of barrier heights l are chosen from the region G_0 in the vicinity to the transition into the region G_-, *i.e.*, in the vicinity to classical homoclinic tangle. Barrier height l is in units of $\frac{U}{\omega'}$.

as

$$\begin{aligned}\mathscr{R}_{2n+1} &= \frac{1}{l}\{a_{2n+1}(l) - \langle ce_{2n+1}(l,\varphi)|V(l,\varphi)|ce_{2n+1}(l,\varphi)\rangle\} \\ &= \frac{1}{l}a_{2n+1}(l) - \frac{1}{4}\sum_{r=0}^{\infty} A_{2r+1}^{2m+1}\left(A_{2r+3}^{2m+1} + A_{2r-1}^{2m+1}\right). \end{aligned} \tag{2.96}$$

Here $V(l,\varphi) = 2l\cos 2\varphi$ and $a_{2n+1}(l)$ is the Mathieu characteristic. Direct calculation of the distance from the Homoclinic tangle for the different states (see Fig. 2.11 and Fig. 2.12) shows that $\mathscr{R}_{2n+1}$ is larger for the states with minimal coherence, while the initial mixed states favourable to the generation of coherence belong to the chaotic region.

2.8 Conclusion

The study is focused on a paradigmatic model of NEMS hybrid system: nonlinear oscillator coupled to the spin-1/2 system. Of interest is the spin dynamics in the region where energy spectrum of the system depends on the height of the potential barrier, and contains degenerate and non-degenerate areas corresponding to the different symmetry subgroups.

Varying the height of the potential barrier switches the symmetry subgroup from degenerate to non-degenerate areas. The isolated system is always in a pure state. The open quantum system initially prepared in a pure state evolves through the intermediate mixed state and finally reaches to a pure state. The dynamics of the longitudinal spin component allows for a fast switching for strong coupling between NV spin and NEMS. However, the coupling of the system of NEMS and NV spin to the environment leads to slower switching. We have also investigated the effects of non-Markovian noise originating due to the spin bath ^{13}C nuclei. Investigating the divergence $C(\rho(t)|\rho_d)$ which quantifies the generation of coherence, we find that the generation of coherence through the unitary transformation is efficient if the system is prepared initially in the chaotic region.